# TIME SCALES AND HETEROGENEOUS STRUCTURE IN GEODYNAMIC EARTH MODELS

HANS-PETER BUNGE, MARK A. RICHARDS
CAROLINA LITHGOW-BERTELLONI
JOHN R. BAUMGARDNER, STEPHEN P. GRAND
BARBARA A. ROMANOWICZ

H. - P. Bunge, Institut de Physique du Globe de Paris
Laboratoire de Sismologie, 4 place Jussieu 75252 Paris Cedex 05 FRANCE
tel: (33) 1 44 27 24 72, fax: (33) 1 44 27 38 94, email: bunge@ipgp.jussieu.fr
M. A. Richards, Department of Geology and Geophysics
University of California, Berkeley CA 94720 USA
C. Lithgow-Bertelloni, Department of Geological Sciences
University of Michigan, Ann Arbor MI 48109 USA
J. R. Baumgardner, Theoretical Division
Los Alamos National Laboratory, Los Alamos, NM 87544 USA
S. P. Grand, Department of Geological Sciences
University of Texas, Austin TX 78713 USA
B. A. Romanowicz, Berkeley Seismological Laboratory, and
Department of Geology and Geophysics
University of California, Berkeley, CA 94720

in press *Science*, April 1998

**Computer models of mantle convection constrained by the history of Cenozoic and Mesozoic plate motions explain some deep mantle heterogeneity structures imaged by seismic tomography, especially those related to subduction. They also reveal a 150 million year time scale for generating thermal heterogeneity in the mantle, comparable to the record of plate motion reconstructions, so that the problem of unknown initial conditions can be overcome. The pattern of lowermost mantle structure at the core-mantle boundary is controlled by subduction history, although seismic tomography reveals intense large-scale hot (low-velocity) upwelling features not explicitly predicted by the models.**

Geodynamic Earth models were pioneered by Hager and O'Connell (*1*), who calculated mantle flow by imposing present-day plate motions as a surface boundary condition. With the advent of global seismic tomography (*2*), these models were extended to predict the geoid and dynamic topography (*3*). However, these Earth models are "static", because they solve for instantaneous mantle flow in response to boundary conditions or internal loads (or both).

Time-dependent Earth models are needed to understand how the evolution of mantle flow affects Earth processes that occur on geologic time scales. For example, continental shelf and platform stratigraphy are controlled by vertical motions of the continental lithosphere in response to mantle convection (*4*). True polar wandering is caused by changes in the inertia tensor due to mantle convection (*5*), and the alternation between periods of rapid and slow magnetic field reversals is probably related to mantle-controlled changes at the core-mantle boundary (CMB).

The development of time-dependent Earth models has been delayed for several reasons: (i) Sufficient compute power to resolve the narrow thermal boundary layers in global mantle convection models has not been available. (ii) It is not obvious how to relate the internal mantle density structure to plate motion observations at the surface, and (iii) we don't know how to initialize time-dependent Earth models at some starting point in the past, because the mantle density structure is only known for the present-day (*6*).

Some of these difficulties have been overcome. (i) Advances in compute power allow us to simulate three-dimensional (3D) spherical convection at a resolution of the order of 50-100 km (*7, 8*). At the same time large-scale mantle velocity heterogeneity structure has been mapped in greater detail (*12, 13*), and seismic tomography has imaged subducted slabs (*9-11*). (ii) The connection of internal mantle density structure to the history of subduction (*14, 15*) has al-

lowed us to estimate the internal buoyancy forces that drive plates (*16*). These developments allow us to combine convection models and plate motion reconstructions, and to test such models with seismic data.

Figure 1b shows an Earth model obtained using the TERRA convection code (*17, 18*). More than 10 million finite elements provide an element resolution of about 50 km throughout the mantle allowing us to model convection at a Rayleigh number of $10^8$ (*19*). The history of plate motion is imposed as a time-dependent velocity boundary condition (*20*) starting in the mid-Mesozoic at 119-100 Million years (Ma). We choose this starting time, because well constrained reconstructions exist only as far back in time as the 119-100 Ma period.

In computing the Earth model (see Table 1) we assume that (i) the mantle is of uniform chemical composition, and (ii) heated primarily from within by radioactivity, with a modest 20 percent component of bottom heating from an isothermal core. (iii) Viscosity increases by a factor of 40 in the lower mantle and in the lithosphere (*21*) relative to the asthenosphere. (iv) Mantle minerals undergo two phase transitions at 410 and 670 km depth. (v) The CMB supports no shear stresses. (vi) The motion of the upper boundary layer can be deduced from plate motion reconstructions. (vii) The initial condition for thermal heterogeneity in the mantle is approximated by a quasi steady-state of convection derived by imposing mid-Mesozoic plate motions for all time prior to 119 Ma.

The first six assumptions roughly constitute a "standard model" for whole mantle convection (*22*). An internally-heated mantle is consistent with cosmochemical and geochemical constraints on abundances of radioactive elements in the mantle (*23*), but a larger component of core heating is certainly possible. Both post-glacial rebound and geoid modeling suggest between one and two orders of magnitude viscosity increase from the upper to lower mantle (*24, 25*).

Our seventh assumption is the most problematic, so we tested how mantle convection responds to a realistic change in plate movement. We first imposed 119-100 Ma plate motions for 2 Billion years to produce an initial condition (Fig.1A). We then imposed present-day plate motions for 500 Ma. The global cross-correlation of the evolving mantle temperature field with the initial condition starts from exactly one [perfect correlation, (Fig.2)] and evolves toward a final stage, at which nearly all initial condition information is lost. Most of the adjustment occurs during the first 150 Ma, and the correlation falls to about 0.3. It drops to a value of about 0.2 in the remaining 350 Ma, which reflects the correlation of the Mesozoic and the present-day plate configuration. Note that the CMB correlation also declines rapidly to about 0.4 during the initial 150 Ma, accelerated by our inclusion of about 20 percent core heating (*26, 18*).

The modeled response time of 150 Ma is comparable to the vertical transit time in our convection model, that is, the time it takes for thermal disturbances to be advected from the surface plates to the CMB. Thus our simulation demonstrates that most of the initial condition "information" from past plate motion regimes is lost after about 150 Ma, suggesting that the plate motion record is probably just adequate for modeling the genesis of present-day mantle heterogeneity (*27*).

We compare the Earth model with the seismic shear body-wave velocity structure of Grand (*10*), which is similar to the compressional body-wave study of van der Hilst et al. (*11*), and with the long-period SH study (SAW 12) of Li and Romanowicz (*13*). Convection at 1100 and 2000 km (Figs. 3A and 4A) is dominated by narrow, linear cold downwellings under North America and the Western Pacific due to subduction of the Farallon, Izanagi and Pacific plates. Mantle temperatures away from downwellings are uniform, as expected for mostly internally heated convection. Note that the Farallon slab is displaced eastward relative to the simple model of Ricard et al. (*15*), because of return flow from sub-Pacific

into sub-Atlantic mantle beneath America.

Smaller-scale downwellings away from plate boundaries are the result of boundary layer instabilities beneath slow moving plates such as Africa. However, their role is minor due to the relatively stiff lithosphere and the radial mantle viscosity structure (*28*). There is a lack of active hot upwellings, owing to the small amount of core heating. Near the CMB at 2800 km (Fig 5A) heterogeneity is dominated by large-scale structure as the cold downwellings spread laterally at the CMB.

The body-wave tomography shows narrow, sheet-like downwellings corresponding to old subducted slabs beneath the Americas (Farallon plate), the Tethys and the Western Pacific. There is a prominent low velocity anomaly under Africa. Other mantle regions show minor heterogeneity. The CMB is characterized by broadscale fast velocity anomalies in the circum-Pacific and a very large-amplitude low velocity anomaly beneath Africa. The long-period SH study, which gives a particularly good fit to the non-hydrostatic geoid, agrees in the overall location of these anomalies.

Some characteristics of GEMLAB1 are similar to Grand's S-wave study, but there are important differences. For example, the cold subduction related CMB temperature pattern in GEMLAB1 correlates well the with seismic models, but there are no prominent hot regions with temperatures substantially above the mean. This is expected inside a hot thermal boundary layer and suggests that the very low wave speed anomalies may not represent purely thermal effects. They may, however, result from chemical heterogeneity, which may also help to explain, why some of the low wave speed anomalies are confined to the deeper mantle.

In the mid mantle, the strong endothermic phase change delays the sinking of material through the transition zone, and GEMLAB1 provides a relatively poor match to Grand's image of subducted slabs beneath some weaker subduction systems under South America and the Tethys. We compared GEMLAB1 to an Earth model GEMLAB2 (not shown) without the strong phase transitions, and find that GEMLAB2 provides a much better fit to Grand's study, as evidenced by the spectral heterogeneity plots (Fig 6).

The mid-mantle differences between GEMLAB1 and GEMLAB2 illustrate the effect of model parameter changes (phase transitions in this case), but uncertainties in the plate motion input data may be equally important. For example, our reconstructions indicate considerably more subduction beneath the Northwestern Pacific than is evident in either seismic model. This suggest to explore improved reconstructions in GEMLAB models.

**References**

1. B. H. Hager and R. J. O'Connell, *J. Geophys. Res.*, **84**, 1031 (1979).

2. A. M. Dziewonski, *J. Geophys. Res.*, **89**, 5929 (1984); J. H. Woodhouse and A.M. Dziewonski, *J. Geophys. Res.*, **89**, 5953 (1984); B. H. Hager and R. W. Clayton, in *Mantle convection: plate tectonics and global dynamics*, W. R. Peltier, Ed. (Gordon and Breach, New York 1989), vol 4, chap.9.

3. M. A. Richards and B. H. Hager, *J. Geophys. Res.*, **89**, 5987 (1984); Y. Ricard, L. Fleitout, C. Froidevaux, *Annales Geophysicae*, **2**, 267 (1984).

4. J. X. Mitrovica, C. Beaumont, G. T. Jarvis, *Tectonics*, **8**, 1079 (1989); M. Gurnis, *Nature*, **344**, 754 (1990).

5. Y. Ricard, G. Spada, R. Sabadini, *Geophys. J. Int.* , **113**, 284 (1993).

6. Because heat transport involves diffusion, one cannot run mantle convection models backwards in time from a relatively well-known present-day state, even if one could construct a perfect forward model.

7. P. J. Tackley, D. J. Stevenson, G. A. Glatzmaier, G. Schubert, *Nature* , **361**, 699 (1993).

8. H. - P. Bunge, M. A. Richards, J. R. Baumgardner, *Nature* , **379**, 436 (1996).

9. S. P. Grand, *J. Geophys. Res.* , **99**, 11591 (1994).

10. S. P. Grand, R.D. van der Hilst, S. Widiyantoro, *GSA Today* , **7**, 1 (1997).

11. R. D. van der Hilst, S. Widiyantoro, E. R. Engdahl, *Nature* , **386**, 578 (1997).

12. W. -J. Su, R. L. Woodward, A. M. Dziewonski, *J. Geophys. Res.*, **99**, 6945 (1994); G. Masters, S. Johnson, G. Laske, H. Bolton, *Philos. Trans. R. Soc. London, Ser. A* , **354**, 1385 (1996).

13. X. D. Li and B. Romanowicz, *J. Geophys. Res.* , **101**, 22245 (1996).

14. M. A. Richards and D. C. Engebretson, *Nature* , **355**, 437 (1992).

15. Y. Ricard, M. A. Richards, C. Lithgow-Bertelloni, Y. Le Stunff, *J. Geophys. Res.*, **98**, 21895 (1993).

16. C. Lithgow-Bertelloni and M. A. Richards, *Geophys. Res. Lett.* , **22**, 1317 (1995).

17. H. - P. Bunge and J. R. Baumgardner, *Computers in Physics* , **9**, 207 (1995).

18. H. - P. Bunge, M. A. Richards, J. R. Baumgardner, *J. Geophys. Res.* , **102**, 11991 (1997).

19. The Rayleigh number based on internal heating approaches the dynamical regime of the mantle, which probably convects with an effective Rayleigh number of order $10^8$ to $10^9$.

20. The plate tectonic information consists of 11 plate motion stages ranging back to 119 Ma. During a stage plate motions are relatively constant. Time boundaries correspond to periods of large or sudden changes in plate motions, that is, plate rearrangements. Plate stage information consists of the complete plate boundaries for all the major plates in existence and the Euler rotation vectors of each plate. The first six plate stages (0-10, 10-25, 25-43, 43-48, 48-56 and 56-64 Ma) span the Cenozoic and are based on the global plate boundaries and rotation poles of Gordon and Jurdy (*30*); the remaining five Mesozoic plate stages (64-74, 74-84, 84-94, 94-100 and 100-119) are based on the global compilation of Lithgow-Bertelloni and Richards (*29*). All plate boundaries and rotation poles are in the hotspot reference frame. The inherent uncertainties associated with using plate tectonic information in geodynamic models are described in (*29*). Many of the Mesozoic reconstructions, particularly for plates that have disappeared (Izanagi, Phoenix,

Kula) or are in the process of disappearing (Farallon), are only approximate, especially the positions of subduction zones and to a lesser extent the rotation poles.

21. In the Earth the lithospheric viscosity is many orders of magnitude larger than the viscosity in the upper mantle, but we don't have the numerical capability to resolve such large viscosity contrast. Simulations (*28*) demonstrate that a 20 fold viscosity increase in the lithosphere is sufficient to suppress boundary layer instabilities.

22. G. F. Davies, and M. A. Richards, *J. Geol.* , **100**, 151 (1992).

23. G. J. Wasserburg, G. J. F. MacDonald, F. Hoyle, W. A. Fowler, *Science* , **143**, 465 (1964).

24. J. X. Mitrovica, *J. Geophys. Res.* , **101**, 555 (1996).

25. B. H. Hager and M. A. Richards, *Philos. Trans. R. Soc. London A* , **328**, 309 (1989).

26. This CMB response time is accelerated by a factor of two, relative to a model without core heating.

27. The correspondence of the mantle response time and the time-period for reliable reconstructions is not coincidental: Reconstructions are largely dependent upon the magnetic isochrons of sea-floor spreading, which is limited to the characteristic maximum age for oceanic lithosphere. Simple boundary layer convection theory (*22*) predicts that this characteristic boundary layer age should be similar to the vertical transit time for convection. Based on the prediction that advection velocities scale roughly with the logarithm of the viscosity contrast (*18*), the mantle response time is probably accurate within a factor of two.

28. H. - P. Bunge and M. A. Richards, *Geophys. Res. Lett.* , **23**, 2987 (1996).

29. C. Lithgow-Bertelloni and M. A. Richards, *Rev. of Geophys.*, **36**, 72 (1998).

30. R. G. Gordon and D. M. Jurdy, *J. Geophys. Res.* , **91**, 12389 (1986).

31. We thank G. Davies and R. van der Hilst for constructive reviews, J. Painter for supporting the 3D graphics, and the Los Alamos Branch of the Institute of Geophysics and Planetary Physics for continuing support. Computing resources were provided by the Advanced Computing Laboratory of Los Alamos National Laboratory.

**Figure Captions**

**Fig 1** (A) Cut-away of the 3D temperature field for a starting model seen from the Pacific hemisphere. (GEMLAB: Geodynamic Earth Model of Los Alamos and Berkeley). The model was obtained by imposing mid-Mesozoic plate motions until quasi steady-state was reached (see text). Blue is cold, and red is hot. The upper 50 km of the mantle are not displayed in order to show the convective planform. Present-day plate boundaries are drawn for geographic reference. Narrow hot zones near the surface reflect passive mantle upwelling at the Izanagi, Farallon, and Phoenix spreading centers. The prominent cold downwelling in the cross-sectional view results from subduction of the Izanagi and Farallon plates in the Northwestern Pacific. (B) Same as (A) but after the 119 Ma through present-day plate motion record has been imposed. Note that the major difference to (A) lies in the more complicated downwelling structure, which reflects the history of subduction beneath the Northwestern Pacific. (C) Map of plate boundaries for the 119-100 Ma stage. Arrows indicate the direction of plate motion. The arrow length is proportional to the plate speed. The ancient Izanagi (IZA), Farallon (FA) and Phoenix (PH) plates occupy most of the pacific basin. (D) Same as (C) but for the present-day. The Izanagi, Farallon and Phoenix plates have largely disappeared.

**Fig 2** Global cross-correlation of the evolving mantle convection model with the initial condition as a function of time. Correlation is shown separately for the upper, the lower, and the whole mantle, and the CMB. A correlation of one means perfect correlation. Zero means no correlation at all. The model evolves from perfect correlation at the beginning toward a final state corresponding to the present-day velocity boundary conditions. Most of the adjustment occurs within the first 150 Ma. The final correlation value of 0.2 reflects the correlation between the Mesozoic and the present-day plate tectonic regime.

**Fig 3** Maps of demeaned lateral heterogeneity at 1100 km depth. (A) is the standard Earth model GEMLAB1 described in the text. The seismic shear wave models are from Grand (B) and Li and Romanowicz (C). For the convection model blue is cold and red is hot. For the seismic models blue is fast and red is slow.

**Fig 4** Same as (3) but at 2000 km depth.

**Fig 5** Same as (3) but at the CMB.

**Fig 6** Spectral heterogeneity maps (SHM's) for GEMLAB1 (A), and the seismic model of Li and Romanowicz (C) and Grand (D). GEMLAB2 (B) is similar to GEMLAB1, but without the strong phase transitions. RMS spectral amplitude is contoured as a function of non-dimensional mantle depth (surface at the top, CMB at the bottom) and spherical harmonic degree (0-12). Each panel is normalized to the maximum amplitude for that panel, and there are 5 contour intervals. The SHM's show a low degree structure in the upper and lower boundary layer, which gives way to a whiter spectrum in the mid-mantle. In GEMLAB1, there is additional pronounced heterogeneity in the transition zone due to the strong endothermic phase transition at 670 km depth.

**Table 1**

**model parameters**

| | |
|---|---|
| outer shell radius | 6370 km |
| inner shell radius | 3480 km |
| T, surface | $300^o$ K |
| T, CMB | $2800^o$ K |
| $\rho$, surface | 3500 kg $m^{-3}$ |
| $\rho$, CMB | 5568 kg $m^{-3}$ |
| $\alpha$, surface | 4.011 x $10^{-5}$ $K^{-1}$ |
| $\alpha$, CMB | 1.256 x $10^{-5}$ $K^{-1}$ |
| $\eta$ (upper mantle) | 8.0 x $10^{21}$ Pa s |
| $\eta$ (lithosphere and lower mantle) | 40 x $\eta$ upper mantle |
| thermal conductivity k | 6.0 W $m^{-1}$ $K^{-1}$ |
| internal heating rate $Q_{int}$ | 6.0 x $10^{-12}$ W $kg^{-1}$ |
| Heat capacity | 1.134 x $10^3$ J $Kg^{-1}$ $K^{-1}$ |
| $\gamma$, 410 km | 2 MPa $K^{-1}$ |
| $\gamma$, 670 km | -4 MPa $K^{-1}$ |

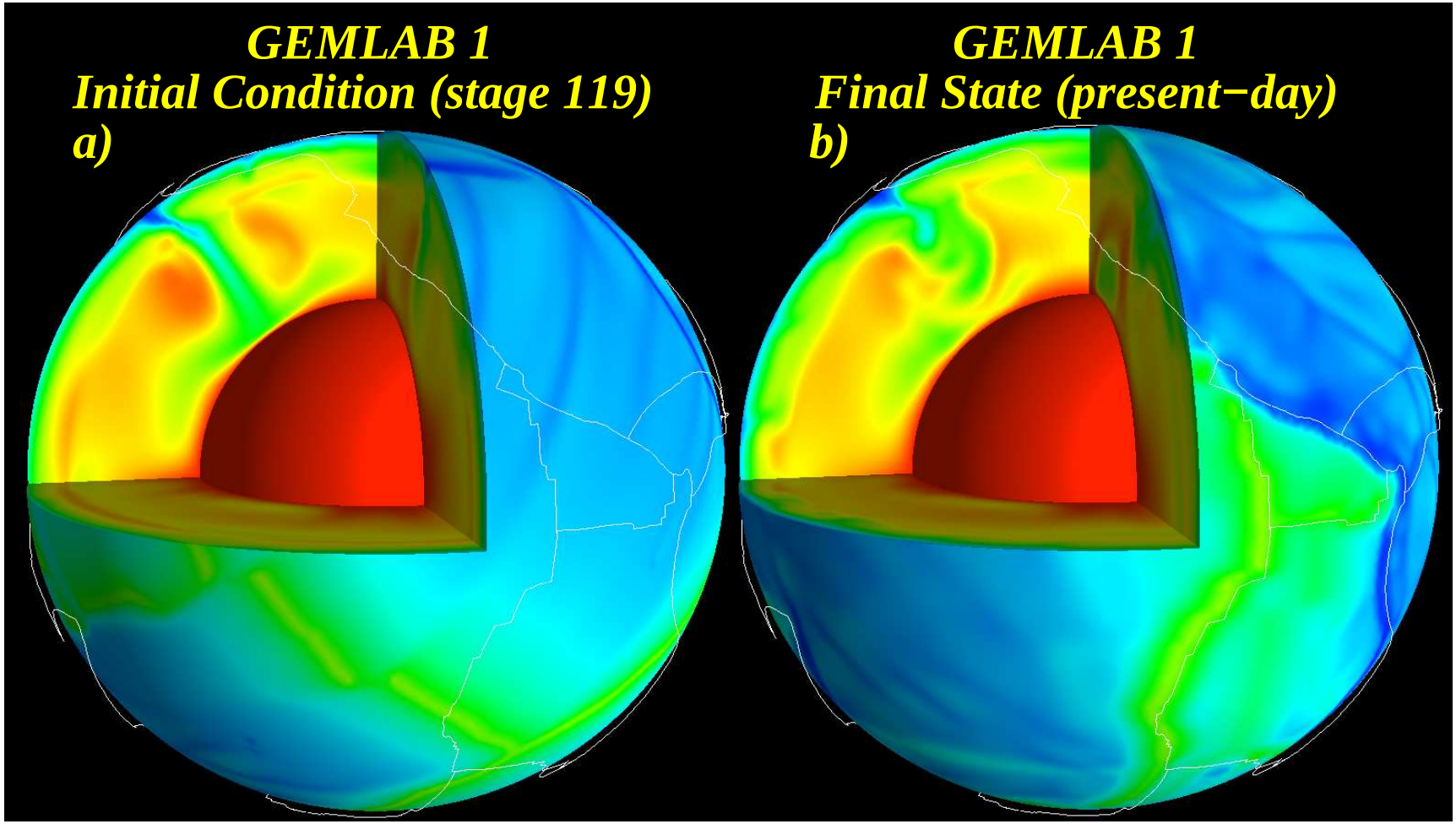


## Observed Plate Velocities

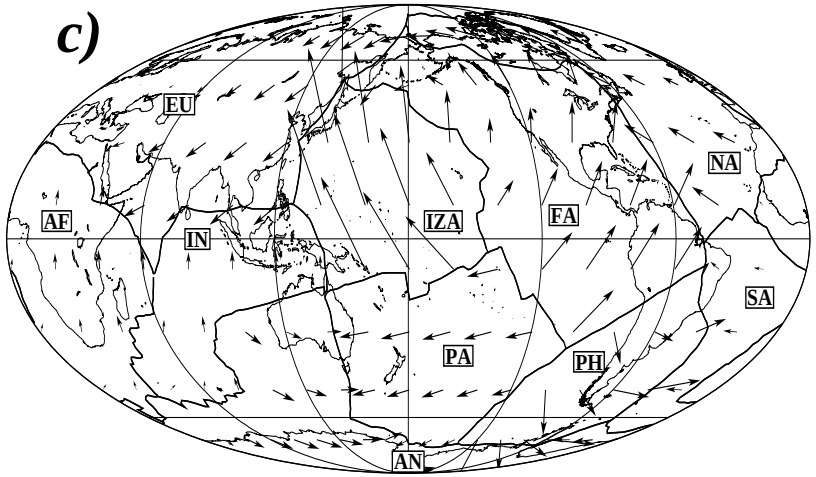


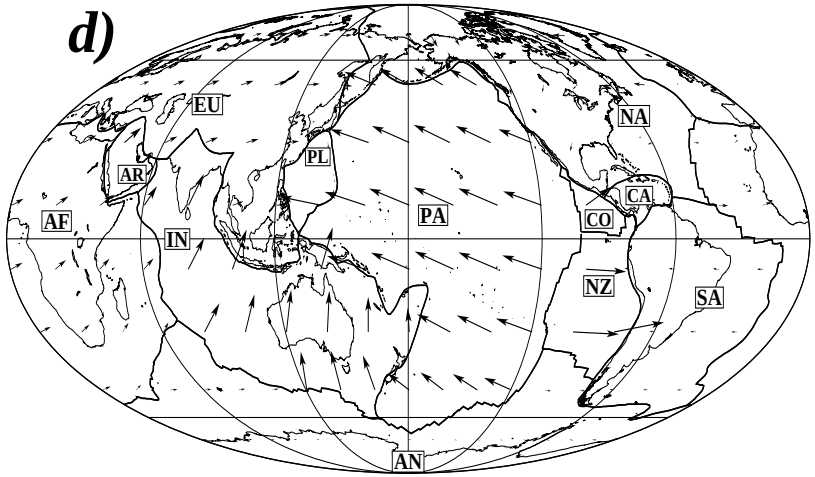

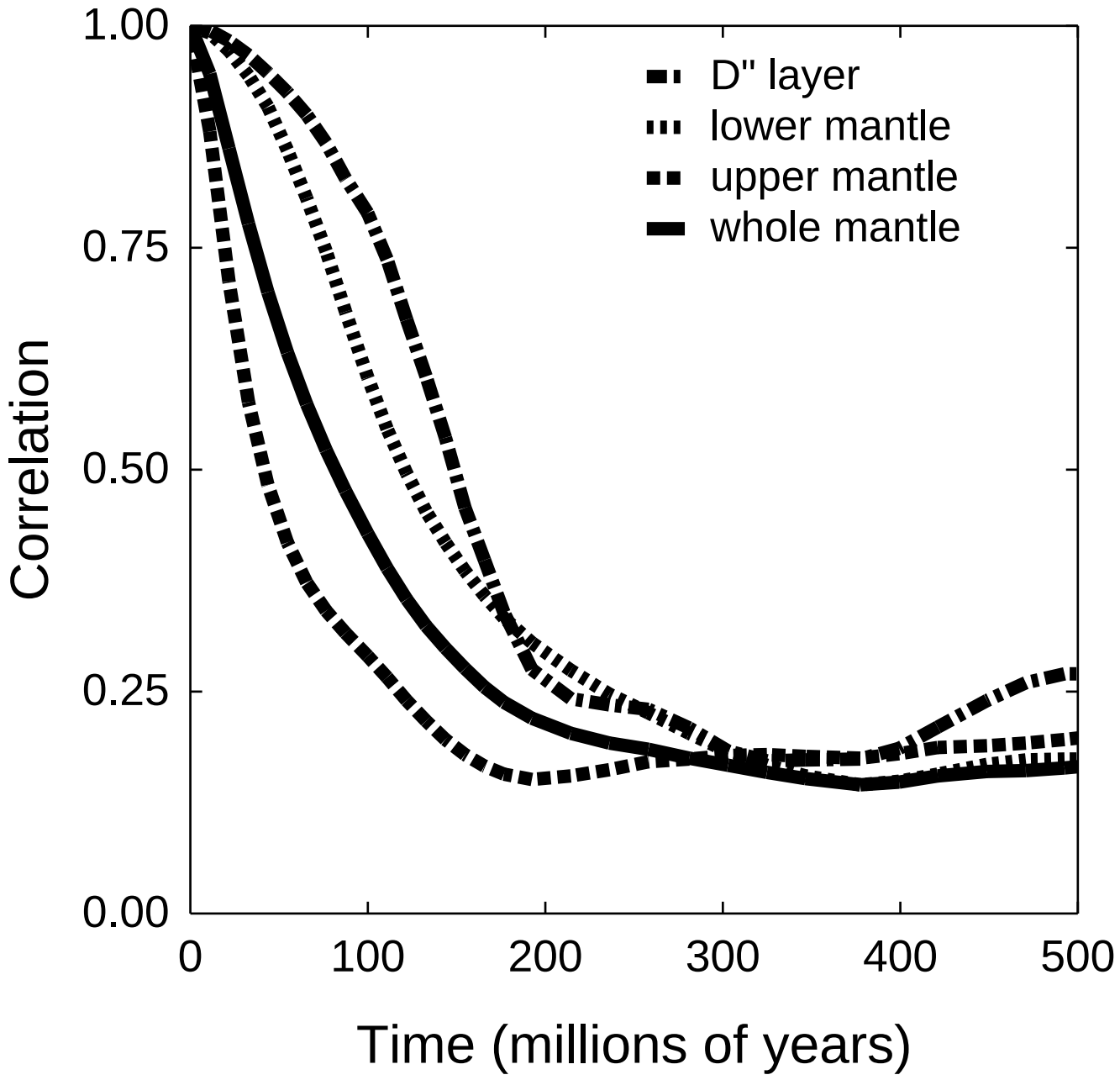
1.00
0.75
0.50
0.25
0.00
Correlation
0
100
200
300
400
500
Time (millions of years)
D" layer
lower mantle
upper mantle
whole mantle

a) GEMLAB 1 (1100 km)

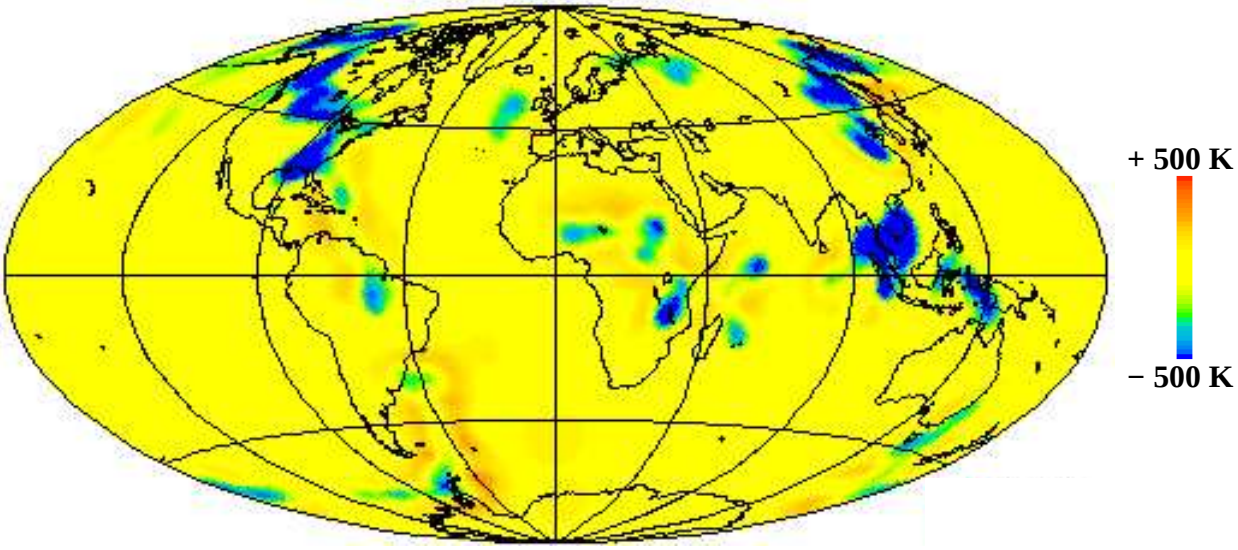


b) GRAND 1997 (1000 km to 1150 km)

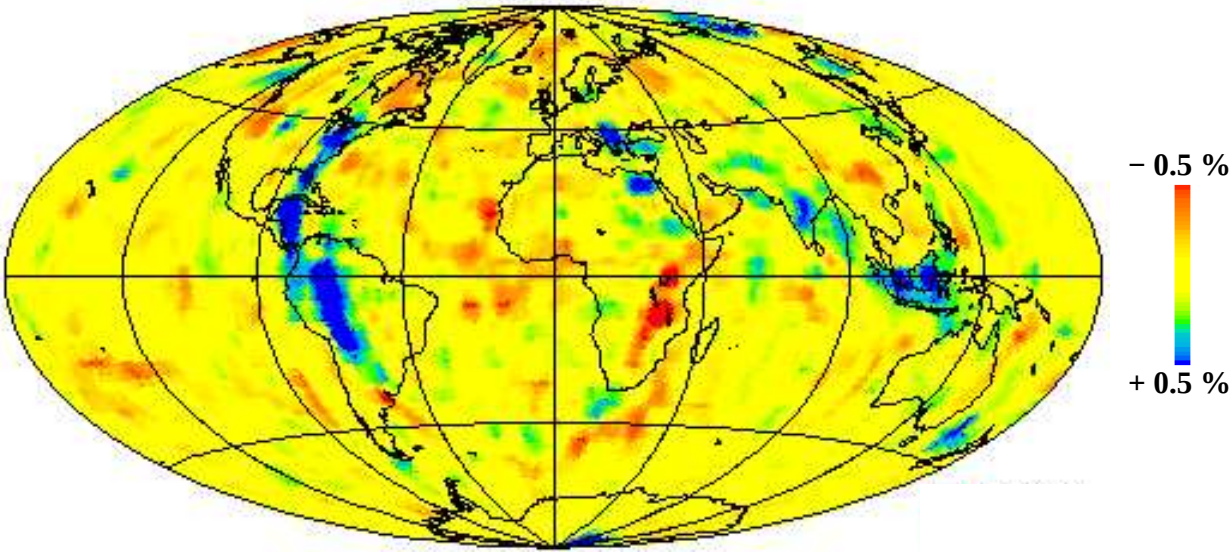


c) SAW 12 (1100 km)

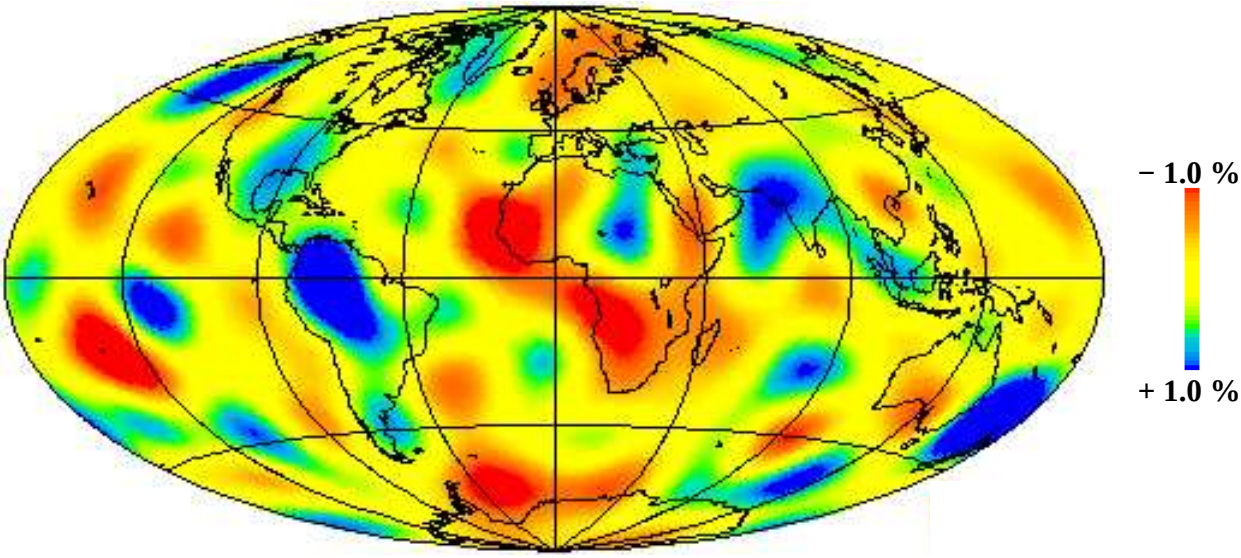

a) GEMLAB 1 (2000 km)

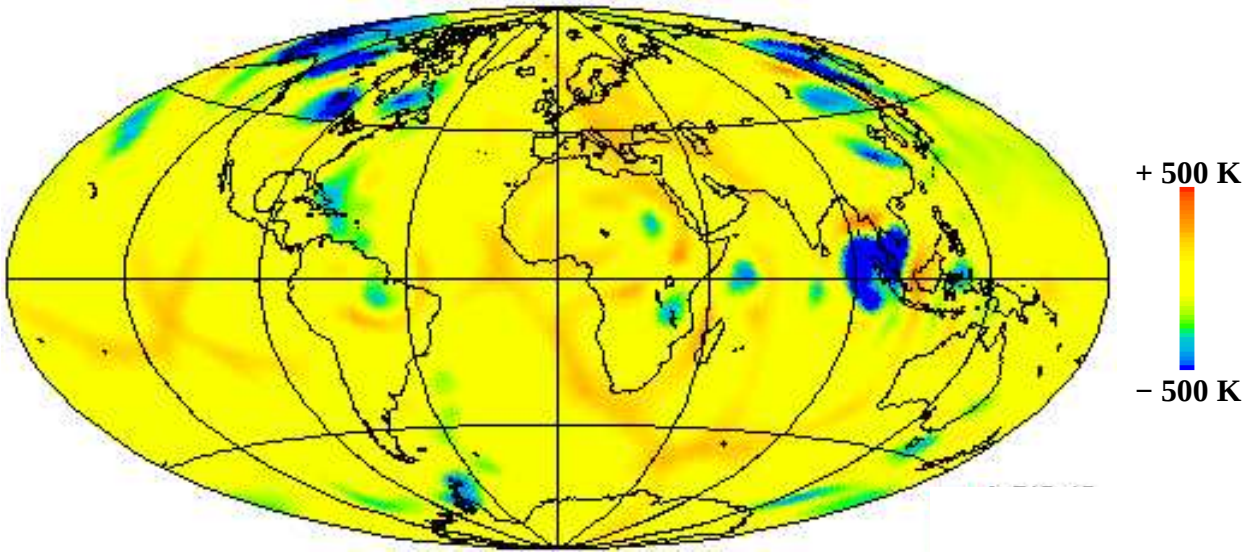


b) GRAND 1997 (1900 km to 2050 km)

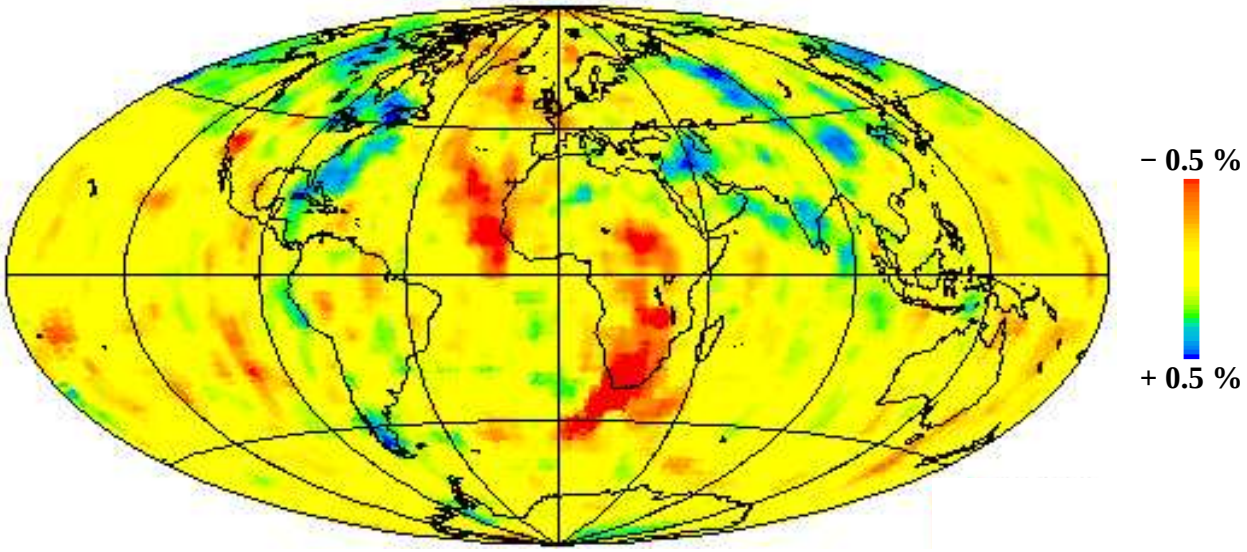


c) SAW 12 (2000 km)

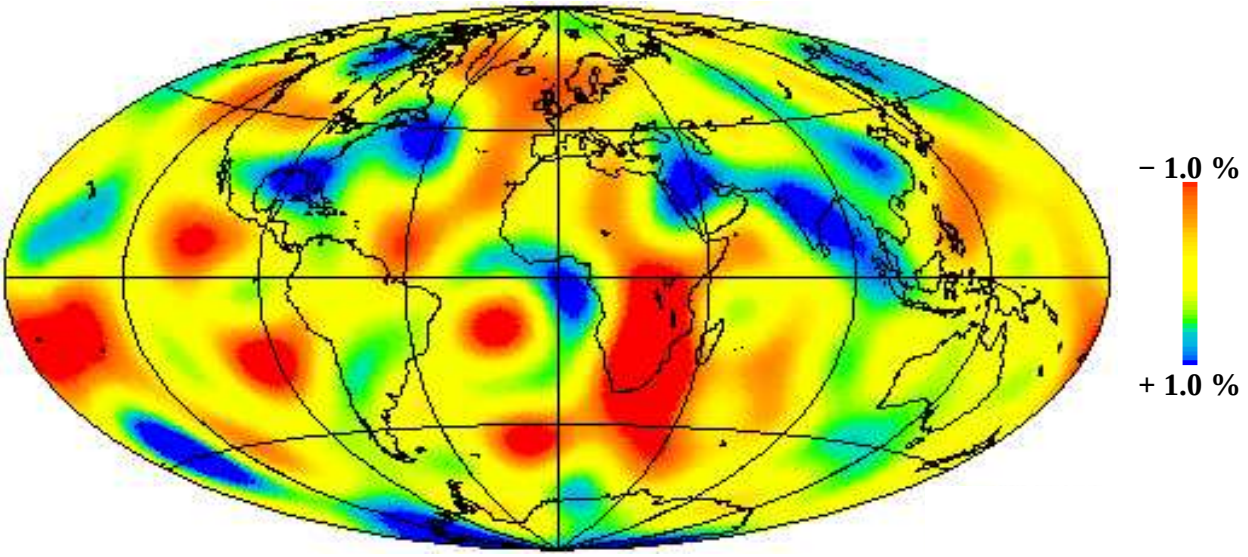

**a)** **GEMLAB 1 (2800 km)**

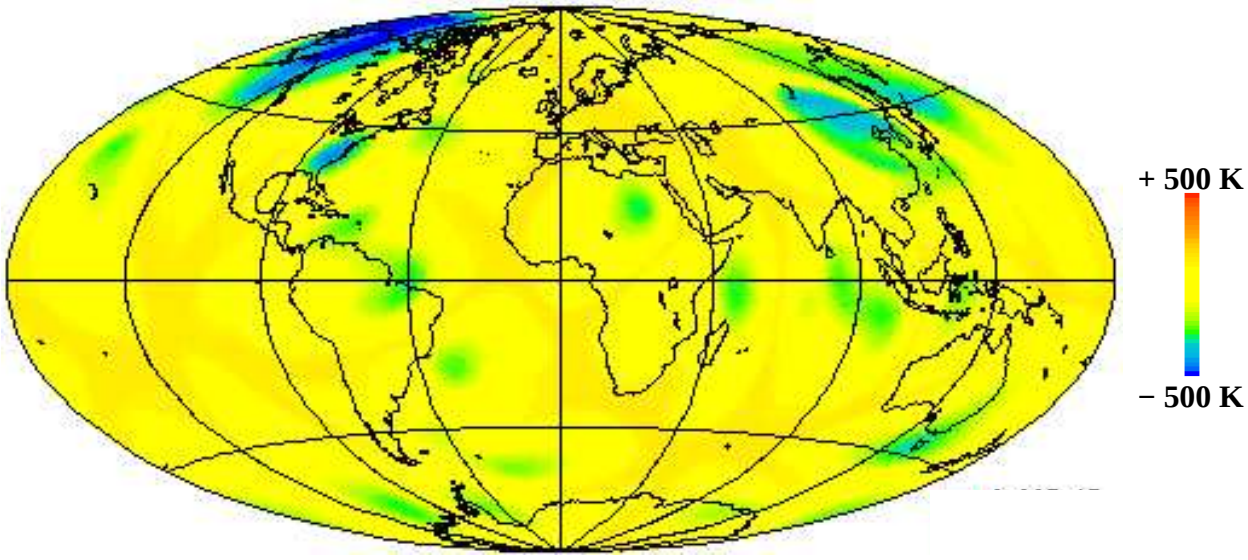


**b)** **GRAND 1997 (2650 km to 2890 km)**

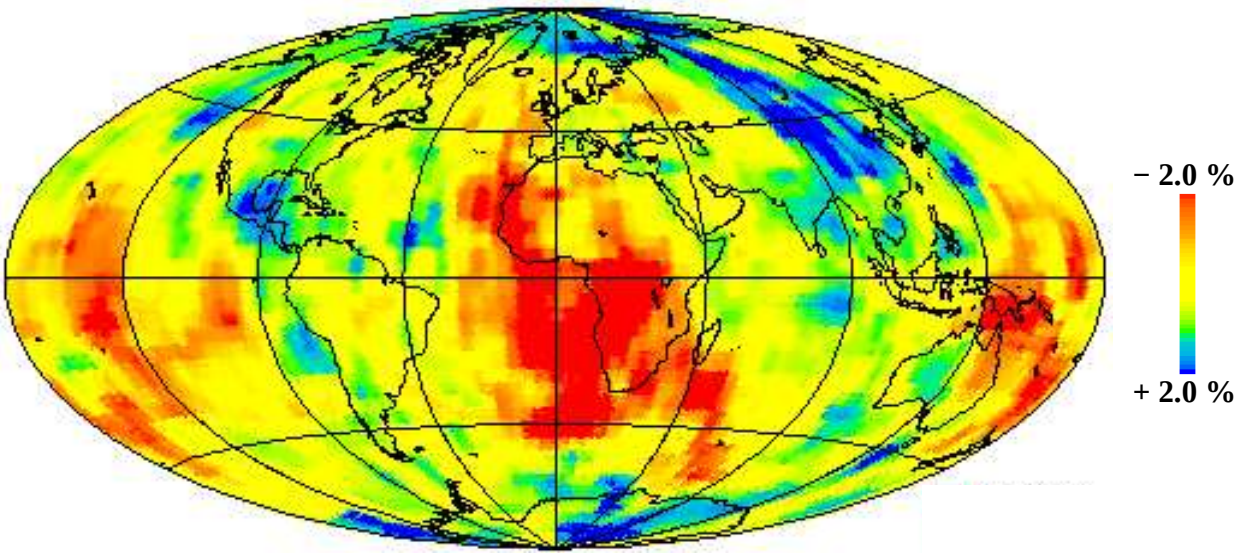


**c)** **SAW 12 (2800 km)**

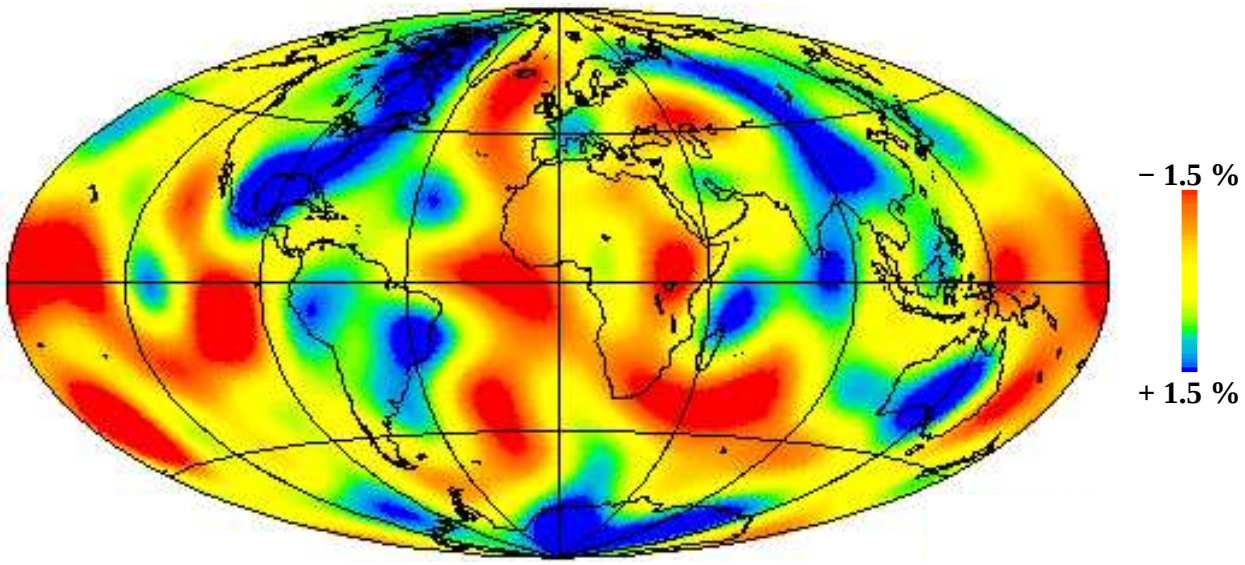

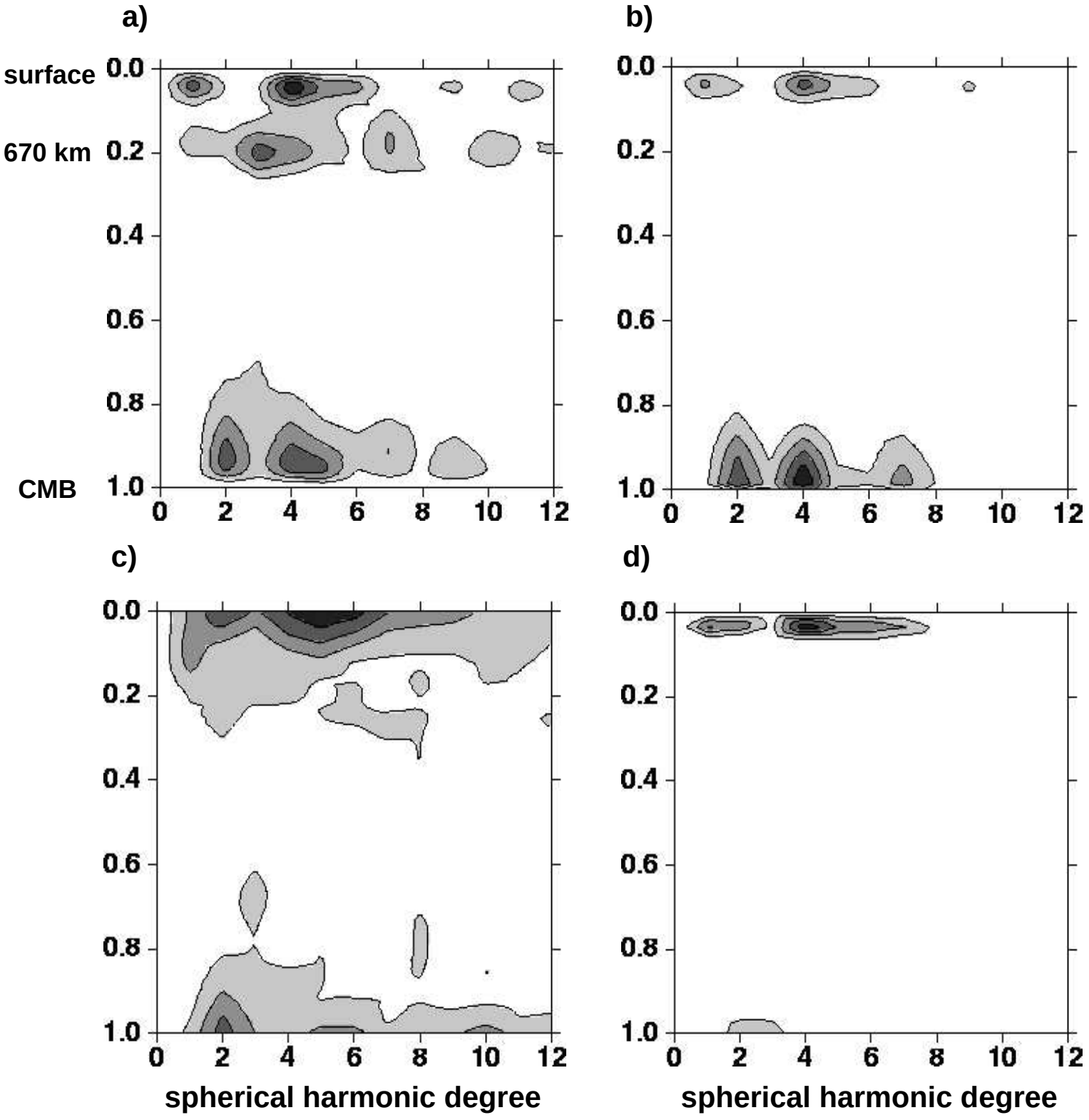
a)
b)
c)
d)
surface
670 km
CMB
0.0
0.2
0.4
0.6
0.8
1.0
0
2
4
6
8
10
12
spherical harmonic degree
spherical harmonic degree